High-Energy Processes in Sources with Relativistic Outflows

Valentí Bosch-Ramon

Facultad de Ciencias Astronómicas y Geofísicas
Universidad Nacional de La Plata
May 8-15, 2013

Outline

Outline

Introduction: high-energy astrophysics

High-energy astrophysics has been developing already for about a century, from both the theoretical and the observational side. Nevertheless, given the limitations in technology and specific knowledge, only until recently it has been possible to carry out systematic studies of the different types of sources that produce very energetic radiation in the Universe:

First, from the 60s-70s, the different areas of research related to high-energy sources have quickly developed firmly sustained in previous seminal or fundamental physics work (relativity, electrodynamics, fluid dynamics and accretion, early non-thermal high-energy physics...), but also thanks to the quick development of instrumentation and computational resources. In addition, during this period, specific theoretical tools have been developed to better explore the high-energy behaviour of astrophysical sources, as it has been done for instance for radiation and dynamical processes.

Moreover, it has been during the last 10 years that many classes of objects have arisen as high-energy sources. All this has been possible thanks to the latest generation of instruments operating mostly at GeV (10^9 eV) and TeV (10^{12} eV) energies. Some of these sources were expected and others were not. Among the expected ones, there is the superclass of sources with relativistic outflows, which comprehends nowadays a good deal of classes and subclasses, both of galactic and extragalactic origin.

Introduction: relativistic outflows

Relativistic outflows are flows of electrons, positrons ($e^{\pm}$) and/or protons (p) and electromagnetic fields.

The bulk of the flow moves relativistically, with speeds well above the *sound speed* **of the plasma.**

Relativistic outflows can be collimated, known as jets, or open, called winds.

These outflows can be produced in different types of objects: active galactic nuclei, collapsing stars of different kind, stellar-mass black holes, and neutron stars. Non-relativistic outflows are also produced in massive stars and young stellar objects.

Being in a low-entropy state, relativistic outflows are prone to dissipate their energy through instabilities, large velocity gradients or magnetic reconnection, leading to heating and the production of ultrarelativistic particles. The presence of highly relativistic particles, $e^{\pm}$ or p, in an environment with dense matter, magnetic and/or radiation fields, usually leads to the generation of emission from radio ($\lambda <$mm) to gamma rays ($E_{\gamma} > m_e c^2$).

In what follows, we will overview the basics of the relativistic outflow phenomenology and physics, focusing in particular on their dynamics and radiation processes.

Introduction: bibliography (I)

General bibliography:

-Aharonian, F. A., 2004, Very High Energy Cosmic Gamma Radiation: A Crucial Window on the Extreme Universe, River Edge, NJ: World Scientific Publishing
-Begelman, M. C., Blandford, R. D., Rees, M. J., 1984, Theory of extragalactic radio sources, Rev. of Mod. Phys., 56, 255
-Bosch-Ramon, V., 2008, Powerful non-thermal emission in black-hole powered sources, Boletín de la Asociación Astronómica Argentina, 51, 293
-Hardee, P. E., 2011, The stability of astrophysical jets, Proceedings of the International Astronomical Union, Symposium S275
-Longair, M., 2011, High-Energy Astrophysics, Cambridge University Press, Cambridge
-Pacholczyk, A. G., 1970, Radio astrophysics. Nonthermal processes in galactic and extragalactic sources, Series of Books in Astronomy and Astrophysics, San Francisco: Freeman
-Rieger, F., Bosch-Ramon, V., Duffy, P. 2007, Fermi acceleration in astrophysical jets, Astrophysics and Space Science, 309, 119
-Rybicki, G. B., Lightman, A. P., 2004, Radiative Processes in Astrophysics, Wiley-VCH verlag, Weinheim
-Romero, G. E., Paredes, J. M. 2011, Introducción a la astrofísica relativista, Universitat de Barcelona Press, Barcelona
-Shore, S. N., 2007, An introduction to astrophysical hydrodynamics, Wiley-VCH verlag, Weinheim
-Spruit, H. C., 2009, Theory of magnetically powered jets, The Jet Paradigm - From Microquasars to Quasars, Lect. Notes Phys. 794

(Look for them in ADS at: *http://adsabs.harvard.edu/abstract_service.html*; **look also at astro-ph)**

Introduction: bibliography (II)

Further readings (I):

-Araudo, A. T., Romero, G. E., Bosch-Ramon, V., Paredes, J. M., 2007, Gamma-ray emission from massive young stellar objects, A&A, 476, 1289 (YSO)
-Araudo, A., Bosch-Ramon, V., Romero, G. E., 2010, Gamma rays from cloud penetration at the base of AGN jets, A&A, 522, 97 (AGN)
-Barkov, M. V., Aharonian, F. A., Bosch-Ramon, V., 2010, Gamma-ray Flares from Red Giant/Jet Interactions in Active Galactic Nuclei, ApJ, 724, 1517 (AGN)
-Bordas, P., Bosch-Ramon, V., Paredes, J. M., Perucho, M., 2009, Non-thermal emission from microquasar/ISM interaction, A&A, 497, 325
-Bosch-Ramon, V., 2008, The physics of non-thermal radiation in microquasars, Lecture notes on microquasar non-thermal radiation physics for the First La Plata International School on Astronomy and Geophysics (microquasars)
-Bosch-Ramon, V., Khagulyan, D., 2009, Understanding the Very-High Emission from Microquasars, International Journal of Modern Physics D, 18, 347 (microquasars)
-Bosch-Ramon, V., Romero, G. E., Araudo, A. T., Paredes, J. M., 2010, Massive protostars as gamma-ray sources, A&A, 511, 8 (YSO)
-Bosch-Ramon, V., Perucho, M., Barkov, M. V., 2012, Clouds and red giants interacting with the base of AGN jets, A&A, 539, 69
-Crusius-Watzel, A. R. 1990, Diffusive shock acceleration in the lobes of the Serpens triple radio source, ApJ, 361, L49

Introduction: bibliography (III)

Further readings (II):

-Derishev, E. V.; Aharonian, F. A.; Kocharovsky, V. V.; Kocharovsky, Vl. 2003, Particle acceleration through multiple conversions from a charged into a neutral state and back, Physical Review D, 68, 3003
-Henriksen, R. N., Mirabel, I. F., Ptuskin, V. S., 1991, Bipolar radio sources in star-forming regions?, A&A, 248, 221
-Hubbard, A., Blackman, E. G., 2006, Active galactic nuclei jet mass loading and truncation by stellar winds, MNRAS, 371, 1717
-Komissarov, S. S. 2011, Magnetic acceleration of relativistic jets, Memorie della Societa Astronomica Italiana, 82, 95
-Perucho, M., Bosch-Ramon, V., 2008, On the interaction of microquasar jets with stellar winds, A&A, 482, 917
-Rodríguez, L. F., Moran, J. M., Franco-Hernández, R., Garay, G., Brooks, K. J., Mardones, D., 2008, The Collimated Jet Source in IRAS 16547-4247: Time Variation, Possible Precession, and Upper Limits to the Proper Motions Along the Jet Axis, AJ, 136, 1852
-Vila, G. S., Romero, G. E., Casco, N. A., 2012, An inhomogeneous lepto-hadronic model for the radiation of relativistic jets. Application to XTE J1118+480, A&A, 538, 97
-Zenitani, S., Hoshino, M., 2001, The Generation of Nonthermal Particles in the Relativistic Magnetic Reconnection of Pair Plasmas, ApJ, 562, L63

Outline

Jets and winds: active galactic nuclei

In the center of galaxies, gas and stars dissipate their energy and angular momentum through (dynamical) friction and fall towards the black hole. It happens mostly in certain periods of the galaxy lifetime during major or minor mergers.

By angular momentum conservation, in-falling matter takes the form of a disc surrounded by a hot and tenuous atmosphere or corona, which radiates thermal emission from the infrared to hard X-rays. A large IR-emitting torus made of dust and gas surrounds the whole region, partially obscuring it.

The accretion of matter by a supermassive black hole in the centre of a galaxy can lead to the formation of powerful relativistic jets. Jets produce non-thermal emission in radio, X- and gamma rays.

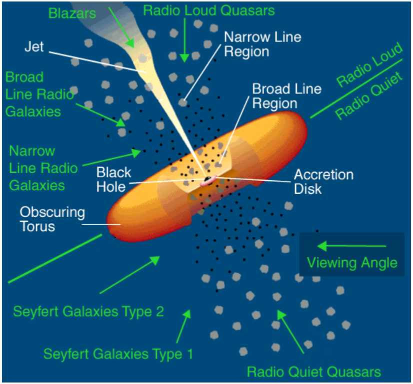

Jet activity is an important element when classifying AGN; geometric factors are also very important, together with accretion rates and black-hole masses.

The jets of active galactic nuclei carry relativistic particles from very close to the black hole, around 100 $R_{\rm Sch}$ to kpc-Mpc distances

The content of AGN jets is still debated. Presently an $e^{\pm}$-jet is favoured very close to the black hole, although normal matter is expected to load the jet when interacting with the medium, from sub-pc to kpc distances.

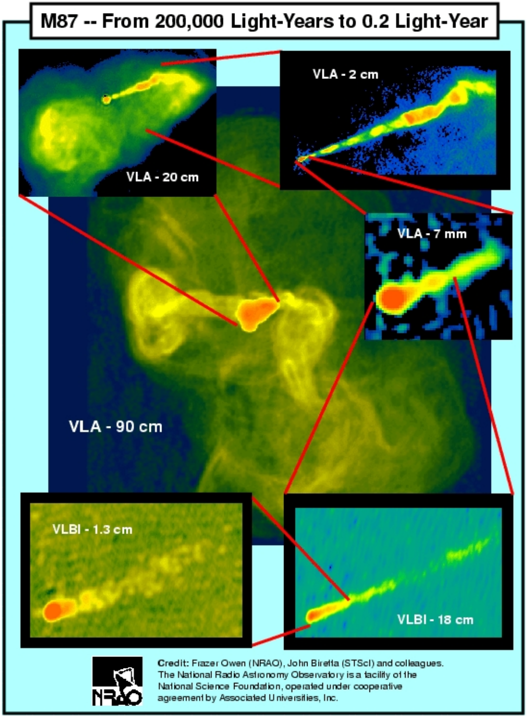

The complex jet of the radio galaxy M87, at $\sim$ 16 Mpc from us. M87 jet apparently had different activity phases in the past, being clearly disrupted at large scales (Fanaroff-Riley I radio galaxy).

Jets have to make their way through the rich environment of the black hole, until eventually reaching the galactic atmosphere, in which they propagate more or less at constant speeds until they terminate because of the inertia of the swept-up medium.

Cygnus A, the first extragalactic radio source detected in 1951, presents (unlike M87) strong signatures of a coherent jet terminating at $\sim$ Mpc from the galaxy (Fanaroff-Riley II radio galaxy).

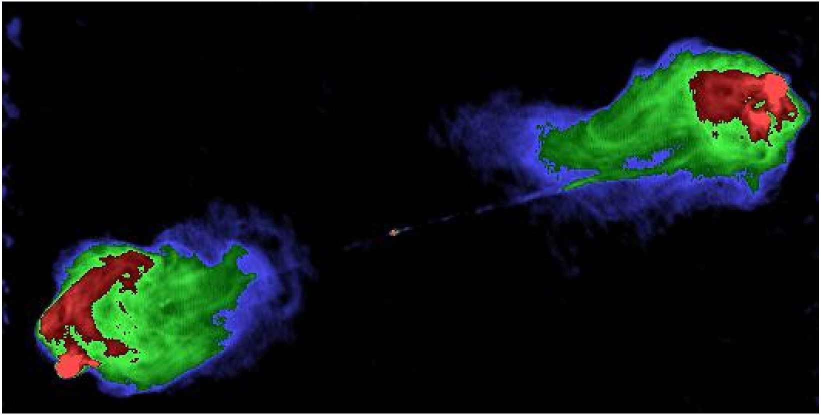

Jets and winds: gamma-ray bursts

Gamma-ray bursts (GRB) are very bright and brief gamma-ray explosions of cosmological origin. This phenomenon was first detected "secretly" in the 60s by US satellites looking for (banned) potential soviet nuclear tests. Their existence was not made public until 1973.

The huge GRB apparent luminosities are explained by the strong collimation of the emitter due to radiation beaming by relativistic kinematics ($\theta \sim 1/\Gamma_{\rm jet}$). In addition, the emitter varies very rapidly, which to avoid causality violation and strong $e^{\pm}$-creation (absorbing gamma rays) requires light retardation effects by $t_{\rm obs} \sim t'/2\Gamma_{\rm jet}$. All together leads to $L_{\rm obs} = \delta^4 L' \approx 16\,\Gamma_{\rm jet}^4 L'$. (shared by all relativistic jet on-axis emission)

Long GRB: A very massive stellar, rapidly rotating, nucleus may collapse directly and very quickly, within one hour, into a black hole, accreting part of the stellar envelop and producing powerful, very relativistic jets visible at cosmological distances. The star must lack the hydrogen external layers to avoid too much jet mass-load. Stars of $M > 40\,M_{\odot}$ may have the required conditions for this phenomenon to take place.

Short GRB: Two neutron stars, or a black hole plus a neutron star, can eventually merge in seconds releasing a powerful beam of matter and radiation, similar but of shorter duration than long GRB.

BURSTING OUT

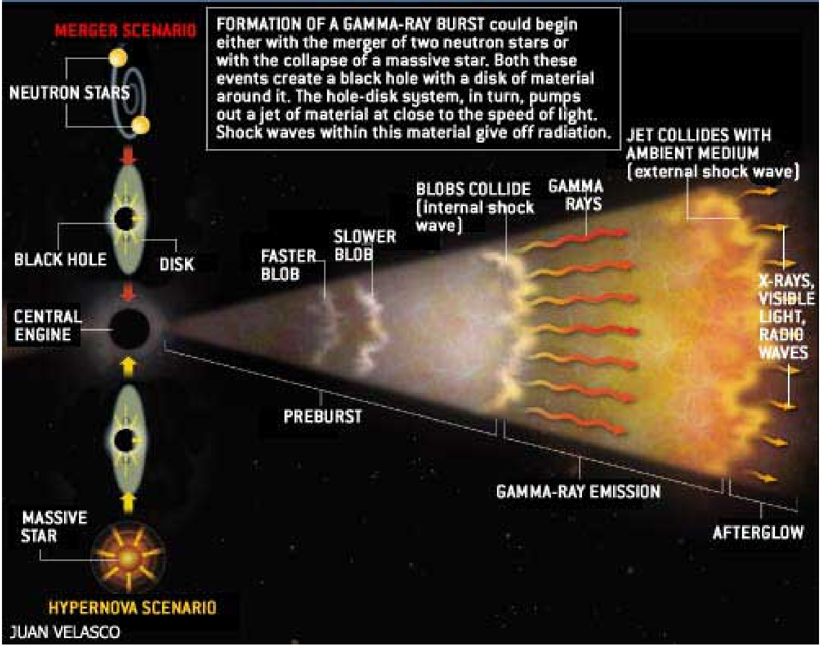

Jets and winds: microquasars

Microquasars host a high- / low-mass, main sequence / evolved star, and a neutron star or a black hole as compact companion. The compact object in these binary systems accretes matter from a stellar companion sometimes forming relativistic jets that produce non-thermal radio emission.

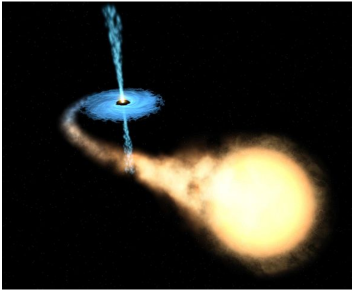

In 1979, collimated outflows were found in radio in SS433, at that time an interesting X-ray and optical source that showed spectroscopic evidence of fast motions. Scorpius X-1 was also a known extended galactic radio source.

In the early 90s, several sources with jets were discovered with strong morphological and kinematic similarities to quasars (quasi-stellar radio sources -an AGN type-), so they were named microquasars.

Artistic image of a microquasar; the star, the accretion disc, and the jets emanating from the compact object.

Since their discovery, several trends have been identified in the microquasar jet/accretion behavior manifested in radio and X-rays mostly but not only; because of the different scales and environment, similarities with AGN and GRB phenomenology and physics are debated.

Jets and winds: microquasars

Accretion discs in X-ray binaries are hotter than in AGN but share the same physics; not quite for GRB, in which accretion is mediated through neutrino cooling instead of electromagnetic radiation.

The jets in microquasars may have a similar origin to those in AGN. However, it is not clear yet whether jets from neutron stars and black holes are fundamentally different.

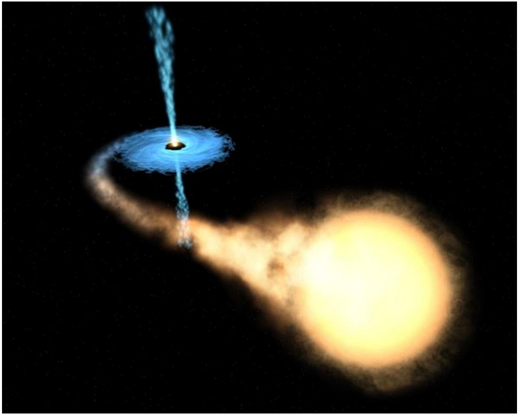

The dominant radiation processes may be the same in the three types of objects, but fundamental details of the non-thermal physics are still unknown, like the particle acceleration mechanism.

Jets and winds: pulsars and their winds

Pulsars, detected as LGM1 in 1967 by Jocelyn Bell Burnell and Antony Hewish, are the first evidence of collapsed objects beyond white dwarfs: neutron stars.

Pulsars rotate with a strong dipolar magnetic field. Charges are generated close to the pulsar surface and within the magnetosphere, and move and radiate along the *B*-lines.

Causality forces the opening of the *B*-lines. An outwards propagating electromagnetic wave is produced that carries away most of the energy and charges ($e^{\pm}$, maybe p and nuclei).

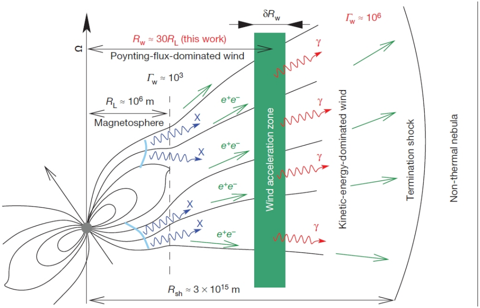

The pulsar wind: generation, propagation and termination

Electromagnetic energy is converted into kinetic energy of a wind that eventually terminates in the surrounding medium.

Jets and winds: pulsars and their winds

Radio/X-ray image of the Crab nebula.

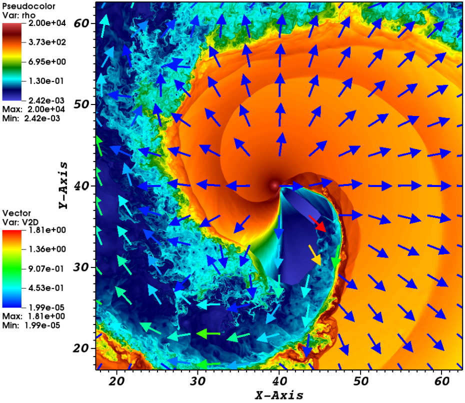

Density in the orbital plane as a result of the interaction between a pulsar and a stellar wind in a binary system.

Pulsars can be found isolated as well as within binary systems. In the former, the pulsar wind termination takes place by interaction with the ISM, whereas the stellar wind and orbital motion are relevant in the latter.

Jets and winds: non-relativistic flows

Stars form through accretion, forming discs that can launch supersonic jets. The jet material suffer collisions with itself and the surrounding medium, brightening through shock-heating. The most powerful and fastest jets are produced by high-mass protostars. For this reason, these are better candidates than low-mass protostars to produce gamma rays that may be detected on Earth.

Massive stars produce powerful winds through radiation pressure. In massive star binaries, the stellar winds collide through strong shocks of great complexity: these shocks are affected by the orbital motion, and are subject to the development of instabilities, which can be enhanced when the shocks are radiative (young pulsars in binaries can lead to similar though more unstable structures than massive star binaries).

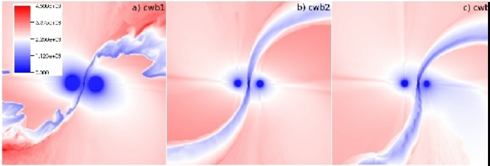

Density in the orbital plane of a colliding wind system.

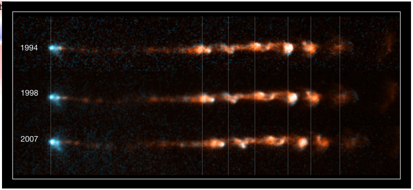

HH 34 in the optical; a young stellar object jet at arcsecond scales.

Outline

Plasma conditions in astrophysical outflows (I)

Because of the low densities, relativistic outflows are typically collisionless plasmas whose particles *know* their way by interacting with the plasma electromagnetic (EM) fields fed by the plasma currents.

Astrophysical plasmas typically fulfill ideal magneto-hydrodynamic (MHD) conditions, i.e. conductivity is infinite: macroscopically the fluid is neutral so in the bulk (collective average) flow frame the electric field vanishes; in a frame with velocity v with respect to the rest frame, charges will *see* $\vec{E} = -\vec{v} \times \vec{B}$.

The flow energy may be dominated by EM fields (force-free electrodynamics), in particular in the outflow formation region, or be shared by the flow bulk motion, thermal motion, turbulence and magnetic field (MHD/HD). Kinetic energy typically dominates in astrophysical outflows far away from the launching point.

Signals in ideal MHD propagate as:

sound waves ($\sqrt{\hat{\Gamma} P/\rho}$): pure isotropic compressional hydrodynamic (HD) wave

alfvenic waves ($\sqrt{B^2/4\pi\rho}$): pure B-field wave; $B_\perp$-fluctuations moving along B-lines

slow magneto-sonic waves: HD + B wave (sound wave along B-lines for high B; alfvenic wave for low B)

fast magneto-sonic waves: HD + B wave (isotropic alfvenic wave for high B; sound wave for low B)

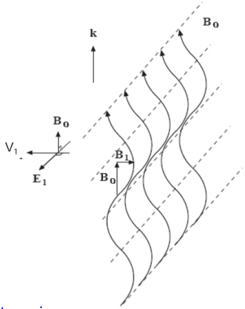

Slow magnetosonic wave

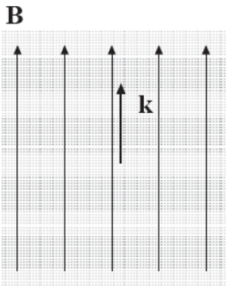

Sound wave

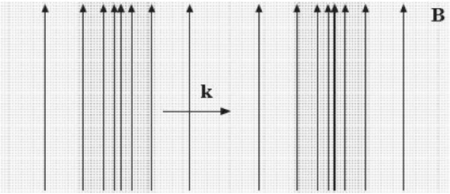

Fast magnetosonic wave

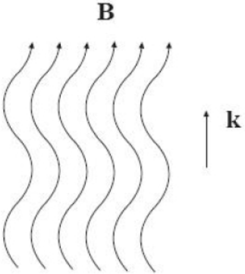

Alfven wave

•

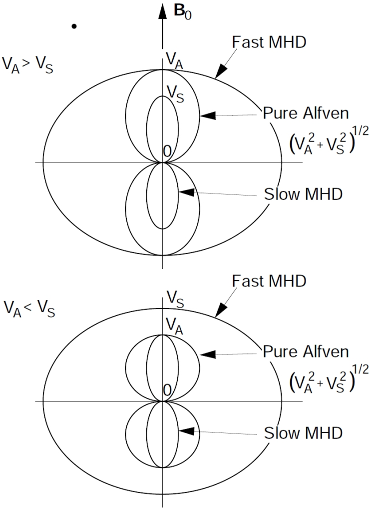

Wave speed versus propagation direction

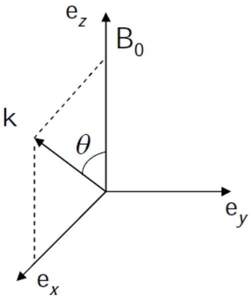

Wave propagation direction

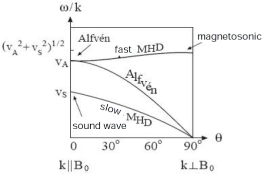

$V_A > V_s$

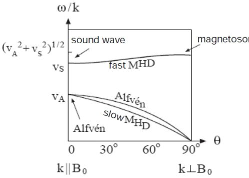

$V_A < V_s$

Wave type with wave direction

Plasma conditions in astrophysical outflows (II)

The formation of a relativistic outflow occurs when matter is accelerated and collimated by the B-field away from the launching point.

Energy dissipation processes take place in the outflows. EM-energy can turn into bulk motion energy through magnetic forces, bulk motion energy into internal energy through shocks, internal energy into bulk motion through a pressure gradient, magnetic/bulk motion into turbulent energy through instabilities...

The Lorentz force $\frac{d(\gamma\, m\, v)_i}{dt} = q\,(\vec{E} + \vec{v} \times \vec{B})_i$ determines the trajectories of charged particles in collisionless plasmas (microscopic scales). It plays an important role in the acceleration of particles, because particles lose/gain energy when getting deflected by plasma receding/approaching B-fields.

Internal energy may be carried by thermal or non-thermal particles, the latter having energies much higher than the plasma average energy in the rest frame of the bulk flow.

The particle gyroradius $r_{\rm g} = E/qB$ is an important quantity that provides a feeling of the particle mean free path in the plasma. The treatment of the plasma as a continuous fluid can be roughly done on scales $\gg < r_{\rm g} >$. Also, to be attached to the plasma, particles must have $r_{\rm g} < l$, being l the typical system size.

(Collisionless) Shocks

Under mild conditions and a weak B-field, perturbations propagate through fluids at the sound speed ($c_s = \sqrt{\hat{\Gamma} P/\rho}$) as waves, in the form of reversible changes of the density and pressure through which the plasma adapts locally to the perturbation propagation. The perturbation energy is quickly shared between fluid elements and *instantaneously* reaches the whole the region.

In astrophysical plasmas, perturbations sometimes propagate faster than the sound speed as shock waves. In this case, energy cannot be transported smoothly, and the process becomes irreversible. The fluid cannot respond collectively to the perturbation, and a substantial fraction of the energy turns into heat through microscopic interactions.

the special case of a strong shock (where the kinetic energy density and kinetic pressure dominate upstream) is simple and instructive. From mass conservation

$$\rho_1 U_1 = \rho_2 U_2 = A$$

where ρ is the mass density, momentum conservation gives

$$A U_1 = A U_2 + P$$

where P is the downstream pressure and energy conservation gives

$$\tfrac{1}{2} A U_1^2 = \tfrac{1}{2} A U_2^2 + U_2 (E+P)$$

$$\Rightarrow \tfrac{1}{2} A (U_1 - U_2)(U_1 + U_2) = U_2 (E+P)$$

$$\Rightarrow P (U_1 + U_2) = 2 U_2 (E+P)$$

$$\Rightarrow r = 1 + \frac{2E}{P}$$

where E is the downstream internal energy density. For a monatomic non-relativistic gas $P = \frac{2}{3} E$ and $r = 4$; for a relativistic gas $P = \frac{1}{3} E$ and $r = 7$. From $U_1 = r U_2$

$$r = U_1/U_2 = \rho_2/\rho_1 = 4\text{: } P_2 = \frac{3}{4} \rho_1 U_1^2 \; (U_1 \ll c)$$

After the passage of the shock wave, the heated and compressed remaining material moves subsonically away from the shock. Within a timescale depending on the nature of the perturbation, continuous or impulsive, the shock will eventually fade away when the shock ram pressure has become similar to the unperturbed medium pressure.

Through microscopic interactions mediated by electromagnetic waves, the shock wave makes the plasma pile and heat up through compression. This occurs too fast to distribute the involved energy and momentum at distances $\gg < r_{\rm g} >$, and the compressed plasma is forced to trail the shock.

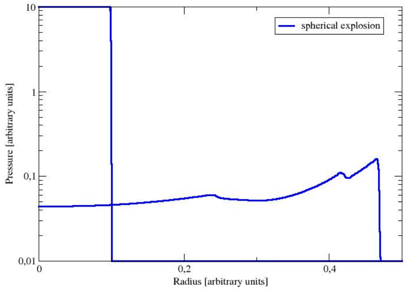

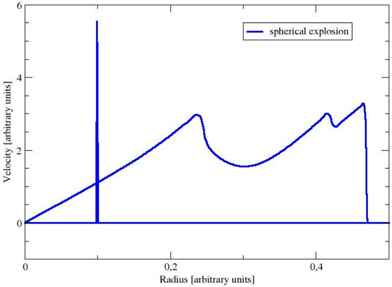

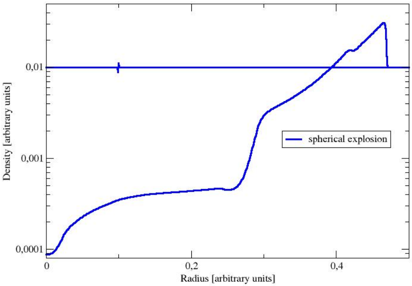

Impulsive injection of energy in a plasma.

In a sound wave, the material does not trail the wave; momentum and energy can be efficiently shared between fluid elements basically without affecting their dynamics.

A cooler and lighter region forms behind the immediate post-shock region. This is a rarefaction wave moving backwards (in the shock frame).

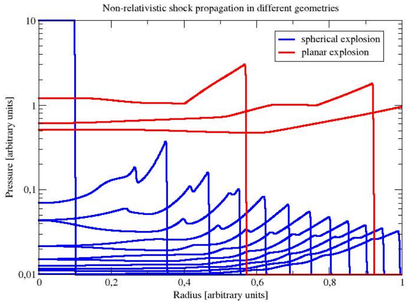

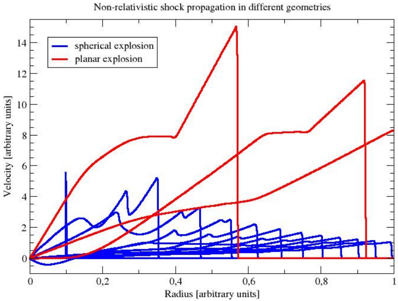

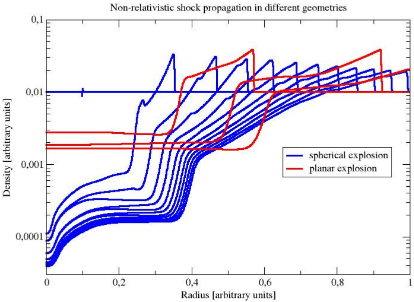

Impulsive injection of energy in a plasma.

Flow stability (I)

Relativistic outflows usually consist of plasma with very low viscosity and supersonic motion: $v \sim c \gg c_{\rm s}$. This means that the plasma Reynolds number, the ratio of inertial to viscous forces, is very large, which in a low-B plasma can be (very crudely) estimated as $Re \sim (c/c_{\rm s})\,(l\,/ < r_{\rm g} >)$, which can be 10^6 or more.

This implies that an initially laminar (supersonic) flow will be prone to suffer hydrodynamic instabilities when perturbed, which will lead to the development of turbulence; i.e. ordered, smaller scale, motions, and also to shocks that will convert kinetic into internal energy.

Under two parallel flows with different velocities, Kelvin-Helmholtz (KH) instabilities develop. Two flows of different densities pressing against each other will develop Rayleigh-Taylor (RT) instabilities. Their typical timescales are of the order of the sound crossing time: $l/c_{\rm s}$; KH grows faster towards smaller scales.

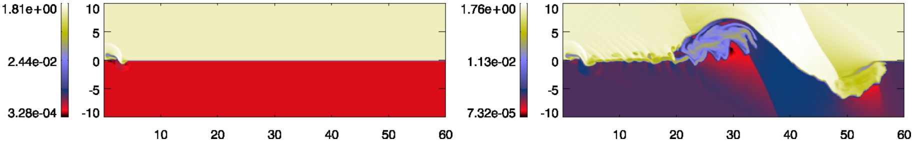

Development of a KH instability at the linear stage.

Flow stability (II)

Kink instabilities are the result of the pinching effect due to a dominant toroidal magnetic field, expected to be dominant in magnetic jets far from the launching region. If the instability grows faster than the jet widens it can disrupt it.

Example of RT (top) and Kink (bottom) instabilities:

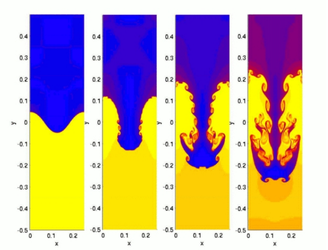

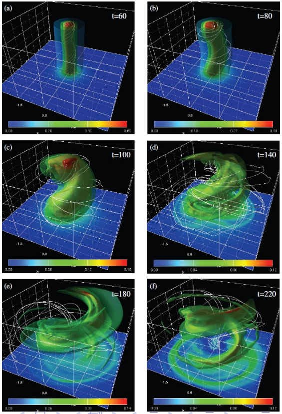

An interesting property of relativistic flows is the development of shocks even under small deviations, because the pressure in the flow frame is P, whereas its ram pressure is $\propto \gamma^2 P$ if $P > \rho' c^2$, so deviations in the momentum flux require lateral pressures of order $\gamma^2 P \gg P$ that trigger strong shocks. For a similar reason, highly relativistic flows tend to be more stable against the development of small-scale disordered (KH) motion.

When the magnetic field becomes dynamically relevant instead of being just a *signal carrier* of the plasma, the development of turbulence becomes more complicated, with anisotropies if the mean B-field is similar or larger than the disordered one.

Outflow production and collimation (I)

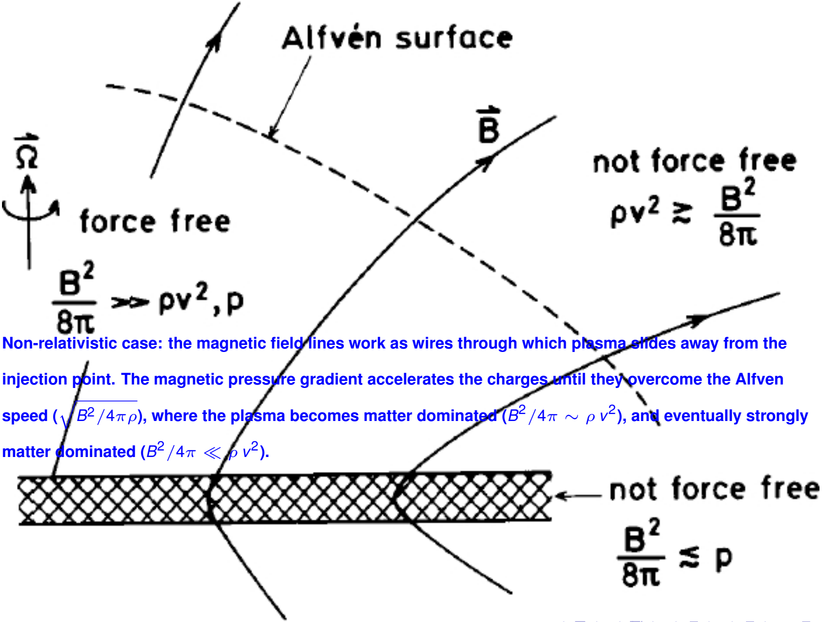

Non-relativistic case: the magnetic field lines work as wires through which plasma slides away from the injection point. The magnetic pressure gradient accelerates the charges until they overcome the Alfven speed ($\sqrt{B^2/4\pi\rho}$), where the plasma becomes matter dominated ($B^2/4\pi \sim \rho v^2$), and eventually strongly matter dominated ($B^2/4\pi \ll \rho v^2$).

Outflow production and collimation (II)

At large distances from the injection point, $B_{\rm r}$ ($\propto 1/r^2$) vanishes and only B_ϕ ($\propto 1/r$) remains, and the flow energetics is expected to be dominated by the flow motion.

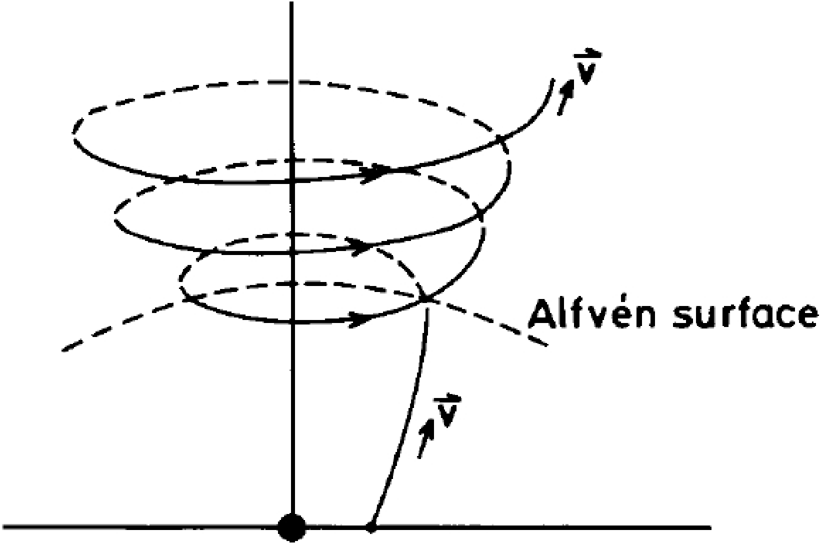

Outflow production and collimation (III)

In magnetic jets, acceleration works until $v_{\rm fm}/v_{\rm j} < \theta_{\rm j}$, point at which the jet becomes causally disconnected.

In non-relativistic magnetic jets, acceleration is achieved when $v_{\rm j} \sim v_{\rm A} = \sqrt{2P_{\rm m}/\rho}$ and $E_{\rm m} \rightarrow E_{\rm k}$. Otherwise, in magnetic relativistic jets, when $v_{\rm j} \sim v_{\rm A}$, $\Gamma_{\rm j} \sim \Gamma_{\rm j\,max}^{1/3}$, constant in a conical jet. To reach $\Gamma_{\rm j} \sim \Gamma_{\rm j\,max}$, the flow lines must diverge faster than the jet expands (i.e. $d\delta r/dz > dr/dz$). A specific profile of external pressure is required to prevent the B-field to open too much.

In any case, it is hard to get $E_{\rm k} > E_{\rm m}$ in 2D stationary jet models. Magnetic instabilities, impulsive magnetic ejections and reconnection may provide with a solution.

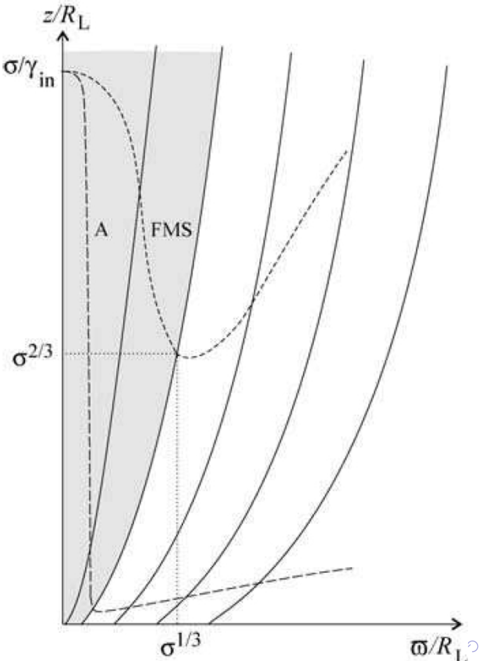

Flow propagation (I)

At some point far from the critical sonic point, the outflow is thought to be kinematically dominated, moving super(magneto)sonically and ballistically. In the case of jets, the surroundings at these scales are the remains of previously ejected material, shocked when pushing external medium.

Ballistic jets expand conically (with $\theta_{\rm j} = \Gamma_{\rm j}^{-1}$ for relativistic jets) until reaching the point where $P_{\rm ext} \sim P_{\rm j}$. There, the jet suffers re-collimation generating an inwards oblique shock or sound wave.

A re-collimation shock and other factors, like hydrodynamical instabilities (Kelvin-Helmholtz) and mass entrainment, can lead to jet disruption. The instability growth is linked to $c_{\rm s}$ at the contact region. For the same $L_{\rm j}$, lighter and faster jets, like those made of $e^{\pm}$-pairs, will need less mass entrainment to slow down because $\dot{M} \propto 1/\Gamma$.

If the flow is powerful and *inertial* enough (it has a large thrust), it will keep more or less laminar until it terminates at the point at which its ram pressure equals that of the external medium in the reference frame of the contact discontinuity.

Flow propagation (II)

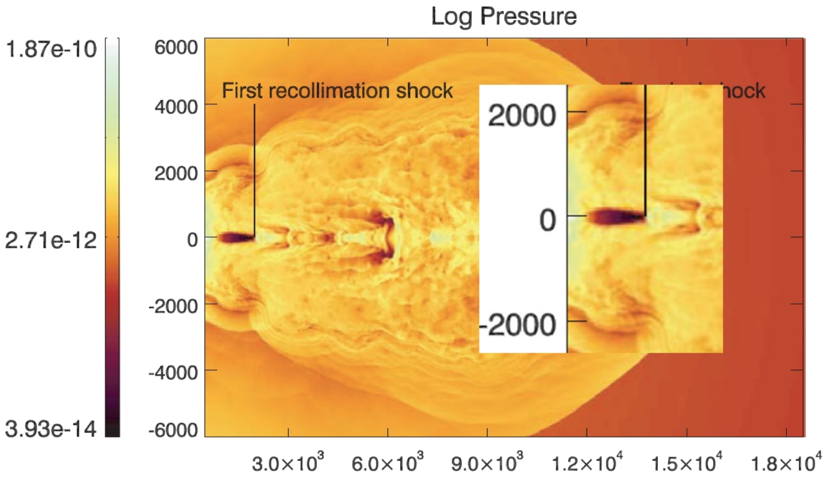

AGN jet freely propagating through the cocoon formed by the jet termination. The free expanding flow is terminated at a re-collimation shock. The cocoon is formed by previously shocked/disrupted jet material.

Flow propagation: colliding winds

A young pulsar orbiting its stellar companion

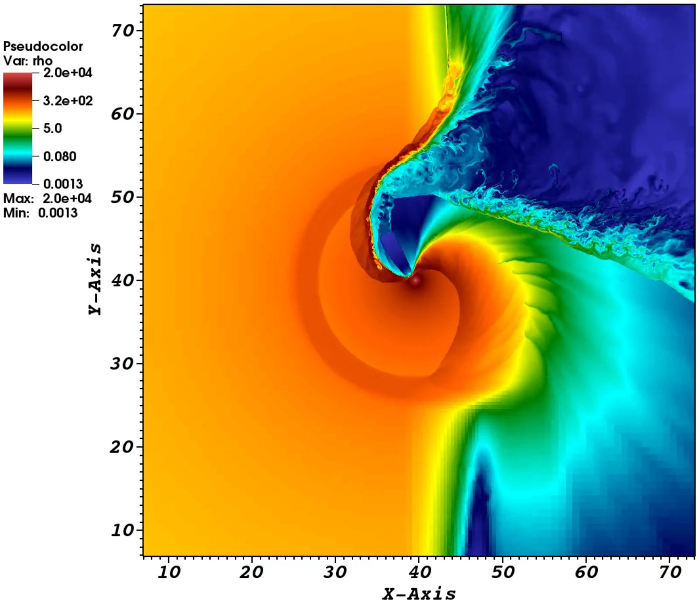

Flow propagation: colliding winds

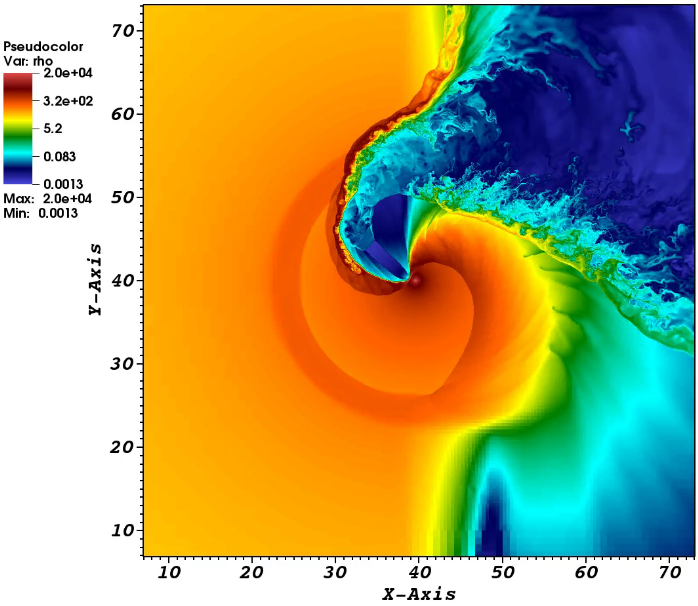

Flow propagation: colliding winds

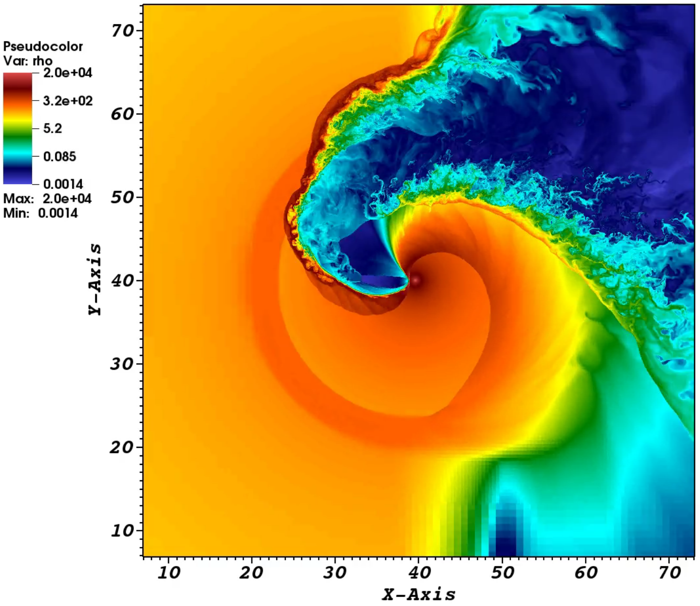

Flow propagation: colliding winds

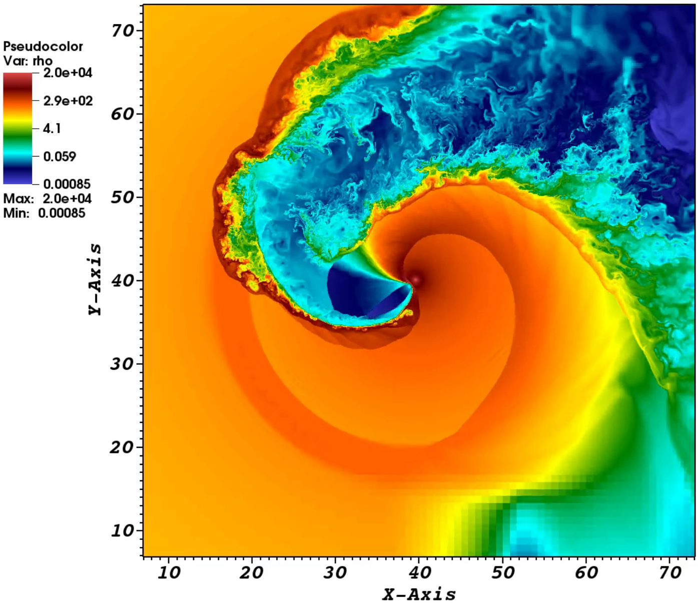

Flow propagation: colliding winds

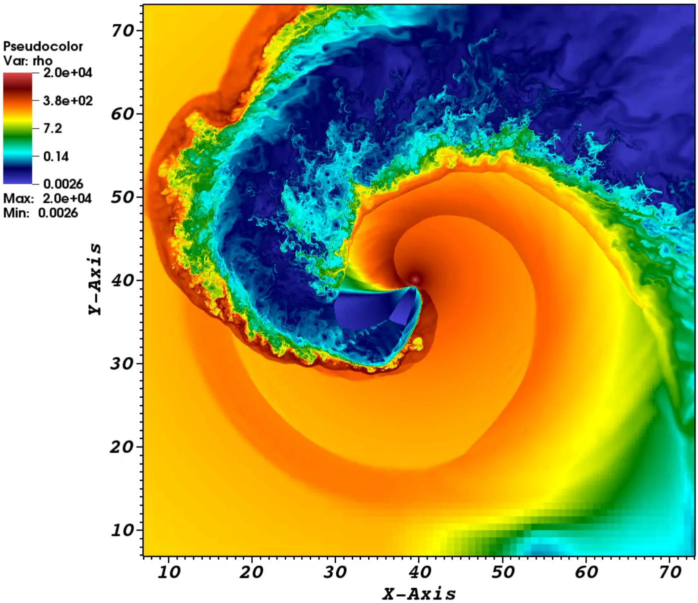

Flow propagation: colliding winds

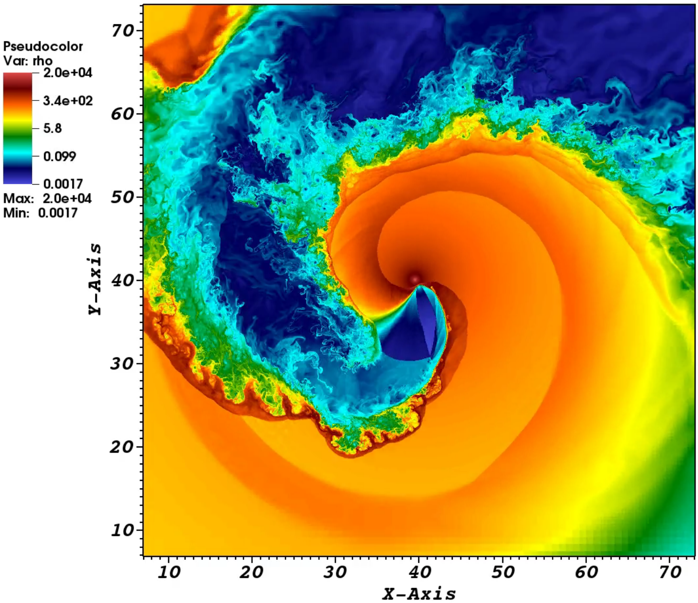

Flow propagation: colliding winds

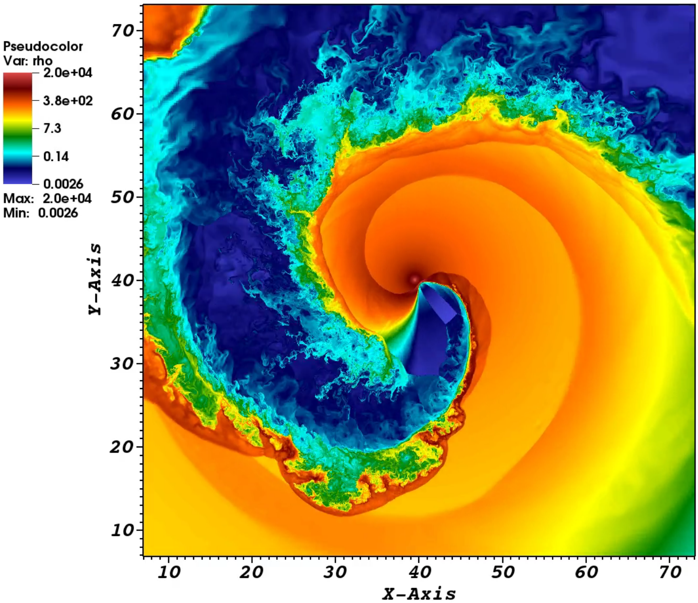

Flow propagation: colliding winds

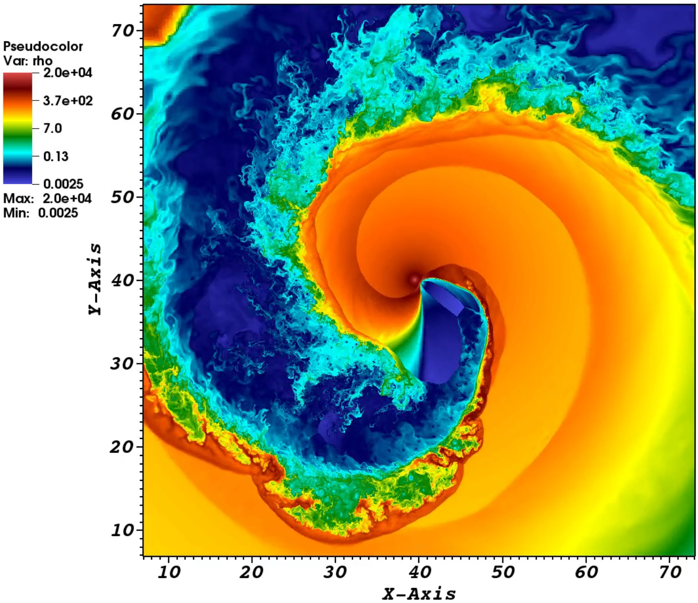

Flow propagation: jet-obstacle interaction

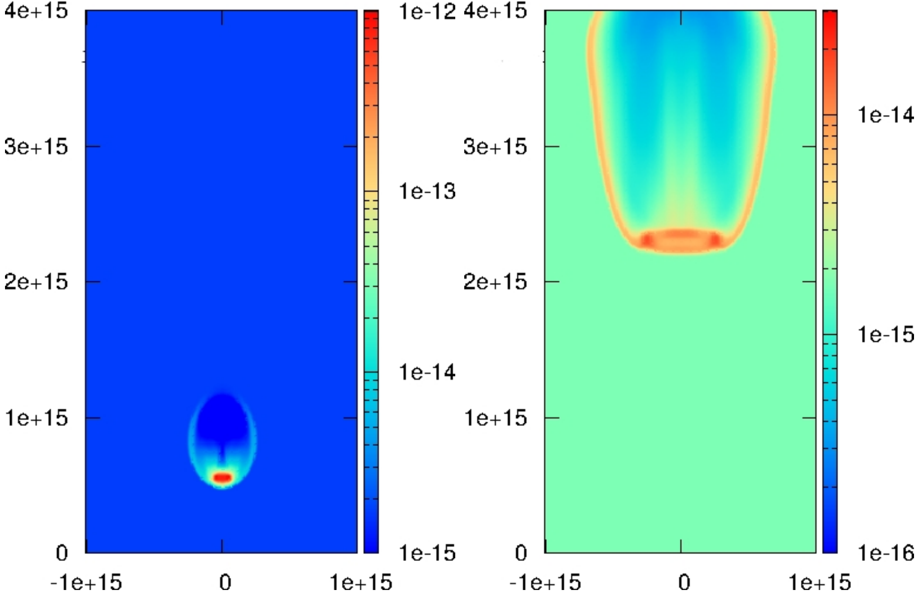

AGN jet interacting with an obstacle, e.g. a lump of matter or the external layers of a red giant. (cgs units)

Flow termination (I)

Initially, the jet head propagates through the environment with a velocity $v_{\rm j}$ driving a strong forward shock in the medium with little energetics because of the small amount of pushed external mass. This is the free propagation phase. The jet section grows, and when $\sigma_{\rm j}\Gamma_{\rm j}^2\rho_{\rm a}\beta^2c^2 \sim L_{\rm j}/c$, the jet head becomes slowed down by the surrounding material.

The flow can suffer disruptive hydrodynamical instabilities linked to the re-collimation shock and the wall contact. If the laminar structure survives the hydrodynamical instabilities, then the jet material reaches through a shock its termination point, filling a hot and diluted cocoon. The cocoon pushes a dense shell of shocked external medium.

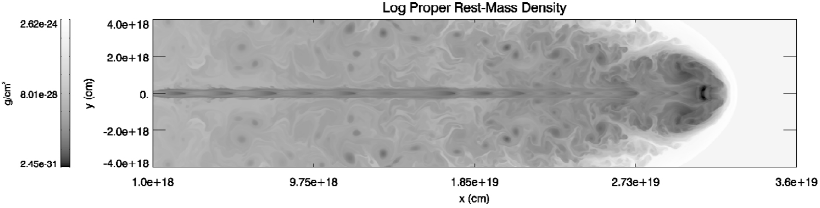

Flow termination (II)

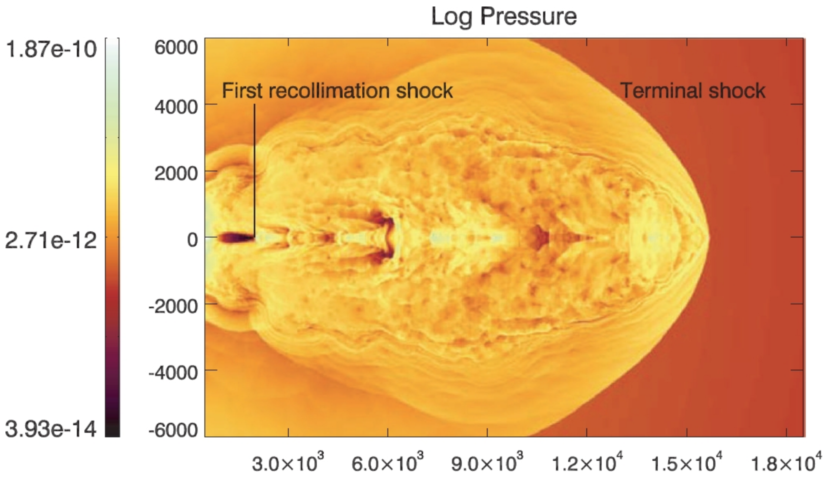

Disruption of an AGN jet due to the impact of a re-collimation shock produced when the jet pressure becomes smaller than that in the surroundings. A shell of shocked IGM can still form.

Flow termination (III)

Some time after fulfilling the condition $\Gamma_j^2 \rho_a \beta^2 c^2 \sim L_j/\sigma_j c$, the jet head slows down with $v \sim (L_j/\rho_a)^{1/5} t^{-2/5}$ in a uniform environment; in the atmosphere of an AGN or in the microquasar surroundings this speed can be $\sim 10^9$ cm s^{-1}. When the jet brakes, a strong shock starts from the jet/medium contact discontinuity moving backwards.

The shocked jet material inflates a hot and diluted bubble, the cocoon, surrounded by a shell of denser and slow shocked medium. At this stage, the jet shares effectively its energy with the environment.

Note that the jet head propagation actually depends on the density profile of its environment, which may be quite different in different types of objects. Eventually, the shock in the external medium gets subsonic.

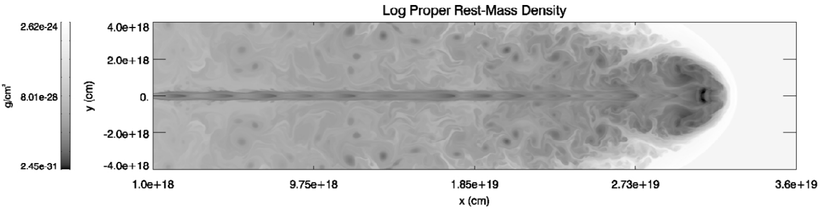

Outline

Dissipation processes and high-energy particles

Magnetic energy is converted into bulk motion (kinetic) energy when the flow is accelerated ($L_{\rm B} \to L_{\rm k}$), and bulk motion energy is converted into internal energy or turbulent motion through shocks and instabilities, with ($L_{\rm k} \to L_{\rm sh,turb}$).

Shocks, turbulent motion and velocity gradients can generate, out of the available kinetic energy, a population of non-thermal particles with $E \gg< E >$. Magnetic energy can go to non-thermal particles also through magnetic reconnection under disordered B-fields and finite conductivity ($L_{\rm sh,turb,B} \to L_{\rm NT}$).

Depending on the dissipation region, different processes may accelerate particles: diffusive shock acceleration (Fermi I), stochastic acceleration (Fermi II), shear acceleration, magnetic reconnection...

Energetic particles of a given gyroradius mainly interact with magnetic structures of size similar to $r_{\rm g}$; i.e. an effective B-field associated to that disorder spatial scale: $B_i(l)$, where $u_{\rm B}^2 \sim \sum B_i(l)^2/8\pi$.

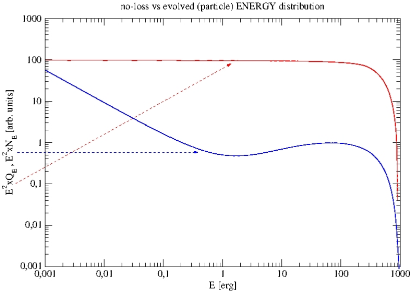

Accelerated particles per energy unit $\times E^2$ (i.e. the energy distribution) multiplied by an arbitrary time and no losses ($E^2 \times Q(E)$), and its counterpart accounting for different types of losses ($E^2 \times N(E)$). The more / less energy in the highest energy range, the harder / softer the distribution is.

Emission in relativistic outflows (I)

The emitter can be the result of self-dissipation, like internal shocks, an external perturbation, like matter clumps or stars, large scale dissipation, due to flow instabilities or velocity gradients (medium-mediated), and the direct interaction with the external medium, through re-collimation or termination shocks.

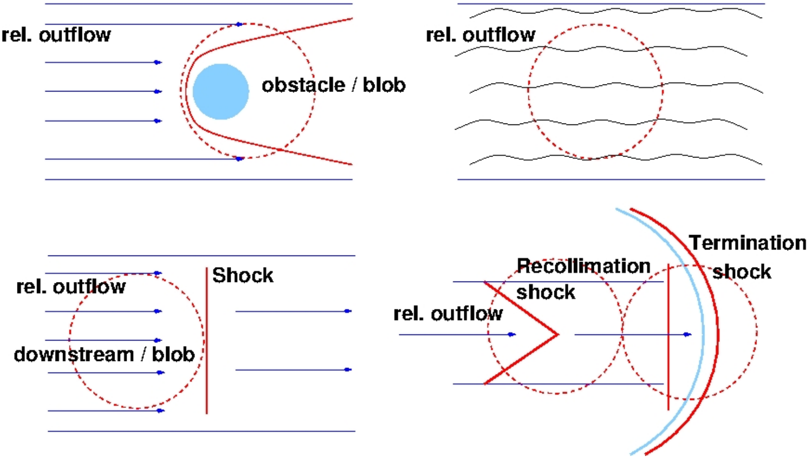

Interaction regions seen from the lab frame

Emission in relativistic outflows (II)

The emitting particle energy distribution $N(E)$ is computed taking into account the acceleration mechanism (sometimes), the cooling (radiative or adiabatic) and escape processes, and the emitter structure (sometimes). Particle transport may be advective or diffusive, and may be 1D–3D. The problem may be time-dependent or stationary.

Particles may be coupled with their own radiation (through reprocessing) or even with themselves (coulombian interactions). If non-thermal particles dominate the energetics of the plasma, the problem becomes strongly non-linear.

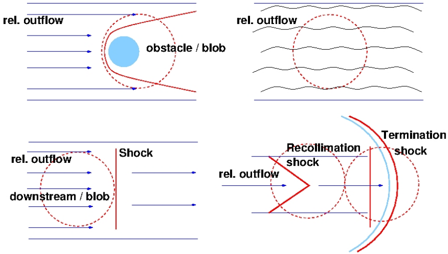

Particles can interact with co-moving targets or with external ones, e.g. at rest in the lab frame.

Phenomenology: radiation in the one-zone model

Sometimes, particles are approximated in the emitter frame as an isotropic population under homogeneous conditions: the one-zone model, described by the following equation ('quantities: emitter frame):

$$\frac{\partial N'\left(t',E'\right)}{\partial t'}+\frac{\partial\left[\dot{E}'(E')N'\left(t',E'\right)\right]}{\partial E'}+\frac{N'\left(t',E'\right)}{t_{\rm esc}}=Q'(E')$$

Each radiation mechanism has a characteristic specific power per particle: $P'_{\nu'}(E')$, and the specific luminosity of a source can be computed from

$L'_{\nu'}=\int_{E'_{\rm min}(\nu')}^{E'_{\rm max}(\nu')}P'_{\nu'}(E')N(E')dE'$.

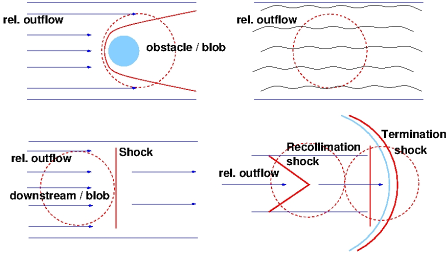

In the observer frame, radiation is to be corrected for Doppler boosting; relativistic kinematic and light retardation effects: $L_\nu=\delta^3L'_{\nu'}$, or $L=\delta^4\int L'_{\nu'}d\nu'$ ($\delta=1/\Gamma(1-\beta\cos\theta_{\rm obs})$; where $\delta\to2\Gamma$ on jet-axis).

Diffusive shock acceleration/Fermi I

Average **charged plasma particles are forced by the** B**-lines to go through the shock and continue downstream. If pressure is dominated by** B**, shock formation is prevented.**

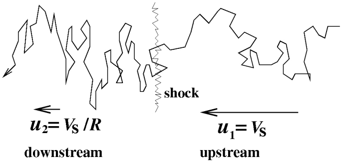

The disordered B**-field, whose irregularities act as scattering centers, allows particles of high enough energy (**$r_g \propto E$**) to diffuse back from the downstream to the upstream region. Diffusion can be considered isotropic in the flow frame in non-relativistic shocks.**

Particles at high energies *see* **the upstream and the downstream regions as converging flows. By bouncing between them, particles gain energy by** $\Delta E/E \propto v_{\rm sh}/c$ **per cycle (for** $v_{\rm sh} \ll c$**), and the acceleration timescale is:**

$t_{\rm acc} = 2\pi (c/v_s)^2\, E/qBc \approx 3\,(0.5\,c/v_s)^2\, E_{\rm TeV}\, B_0^{-1}$ **s**

Collisionless non-relativistic strong shocks with small B**-fields lead to particle energy distributions** $Q(E) \propto E^{-2}$**.**

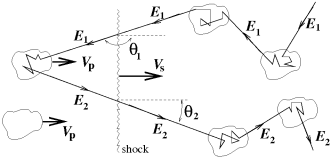

Relativistic shocks present strong anisotropy upstream; $\Delta E/E = \Gamma^2\theta^2/2 \gtrsim 2$**; worse:** $B_\perp$ **is strong downstream: quick turbulence generation is required.**

Stochastic acceleration/Fermi II

Turbulent motions, on average, provide energy to particles through scattering with magnetic irregularities that move through the fluid roughly at the Alfven speed ($v_{\rm A} = \sqrt{B/4\pi\rho}$ for the non-relativistic case).

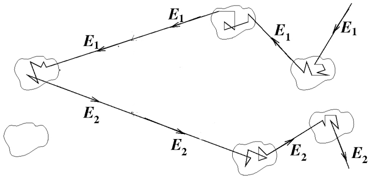

Scattering on B-irregularities provides acceleration that is second order in velocity: $\Delta E/E \propto (v_{\rm A}/c)^2$, with an acceleration timescale (Bohm diff., non-relativistic):
$t_{\rm acc} \sim (c/v_{\rm A})^2\, E/qBc \approx 36\, E_{\rm TeV}\, v_{\rm A9}^{-2}\, B_0^{-1}$ **s**

The accelerated particles follow a $Q(E) \propto E^{-p}$ with $p \lesssim 1.5$ or even Maxwellian-like. The distribution of particles is harder than in Fermi I because of the different acceleration-escape relation and evolution in momentum space.

To be efficient, very strong turbulence is required and particle escape must be slow. In addition, the fluid must not expand, or adiabatic losses will suppress the process.

Shear acceleration

When in a region filled by moving magnetic irregularities there is a strong velocity gradient $\Delta u/\Delta R$, very energetic particles can *see* regions of different velocity, as it happens in shocks. This leads to shear acceleration.

The energy gain (Bohm diffusion; non-relativistic) is $\Delta E/E \propto (\Delta u/\Delta R)^2\, r_{\rm g}^2 \propto E^2$, with an acceleration timescale: $t_{\rm acc} \approx 3(\Delta R)^2/r_{\rm g} c = 300\, B_0\, \Delta R_{11}^2\, E_{\rm TeV}^{-1}$ s

Given that $t_{\rm acc} \propto E^{-1}$, shear acceleration is at least as fast as any other relevant cooling process, so when it works it cannot be stopped until $r_{\rm g} > \Delta R$.

An injection mechanism is needed to get particles with enough $r_{\rm g}$ to *see* the velocity gradient (Fermi I and the converter mechanism -next- have a similar limitation).

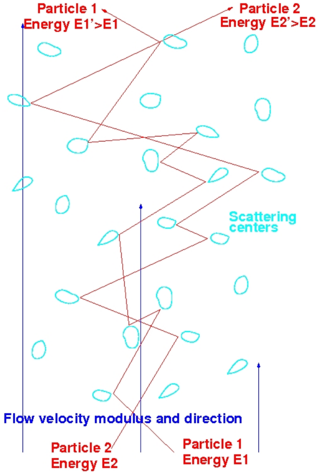

The resulting particle distribution is $Q(E) \propto E^{-(1+\alpha)}$, where α relates the mean free path with the particle energy: $\lambda \propto E^{\alpha}$ (Bohm diffusion: $\lambda \sim r_{\rm g}$ and $\alpha = 1$).

Converter mechanism

In relativistic shocks, $\Delta E/E \sim \Gamma_{\rm sh}^2\, \theta^2/2$, where θ is the angle between the particle velocity and the shock normal. Upstream, B-field deflection allows the shock to catch up with the particle when $\theta \sim 2/\Gamma_{\rm sh}$, so $\Delta E/E$ becomes ~ 2.

Neutral particles will not suffer deflection, so if some fraction of the non-thermal energy is in the form of neutral particles, they will propagate further upstream of the shock. If particles become charged again at a distance $l_0 = 1/(\sigma n_{\rm t}) \sim \Gamma_{\rm sh}^2\, r_{\rm g}$ (where R is the shock front size): $\theta \sim 1$ and $\Delta E/E \sim \Gamma_{\rm sh}^2$.

For efficient acceleration, $\tau^2\Gamma_{\rm sh}^2 \gtrsim 1$, where $\tau \sim \Gamma_{\rm sh} R/l_0$, implying that $l_0 > \Gamma_{\rm sh}^2 R$, when most of particles will escape and $Q(E)$ will strongly soften. The acceleration timescale is now maximal: $t_{\rm acc} \sim r_{\rm g}/c \approx 0.1\, E_{\rm TeV}\, B_0^{-1}$ s.

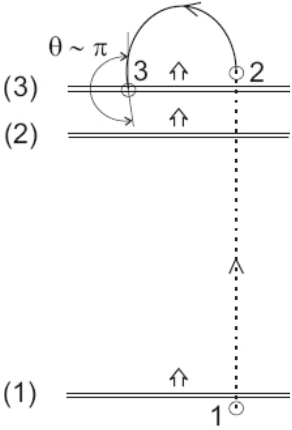

Note that due to the charge-to-neutral conversion particles can cross the relativistic shock from the downstream region despite B-dragging.

Magnetic reconnection

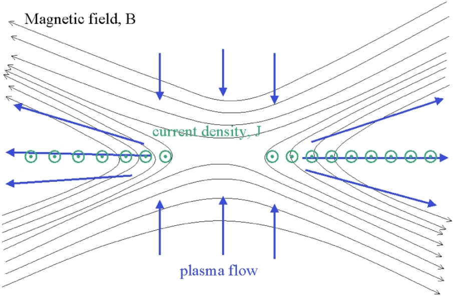

When parallel B-lines of opposite polarity get closer than a certain distance, the plasma currents cannot sustain them (finite conductivity) so they reconnect.

Under normal conditions, reconnection is a slow process unless small-scale turbulence is present, which can enhance the reconnection rate.

Under reconnection, bulk acceleration of the plasma to the initial Alfven speed can be achieved. In this way magnetic energy is converted into kinetic energy.

Particles may be accelerated: (i) by the electric field generated in the reconnection layer; (ii) bouncing between this layer and the incoming flows; or (iii) between the incoming flows themselves, as Fermi I.

Either case, short acceleration timescales are achieved, of order $r_g/c \lesssim t_{acc} \lesssim (v_A/c)\, r_g/c \approx 0.1\,(v_A/c)\, E_{TeV}\, B_0^{-1}$ s

Due to slow escape, an acceleration distribution $Q \propto E^{-1}$ can be achieved in the reconnection region.

Multiple reconnection sites moving randomly in a magnetized turbulent region will lead to Fermi II.

Outline

Relativistic Bremsstrahlung

Accelerated charged particles generate EM pulses mostly $\perp$ to the acceleration in the instantaneous rest frame. The spectrum of the radiation is linked to $\vec{a}(t)$ through its Fourier transform $\vec{a}(\nu)$ as $P_\nu(E) \propto |\vec{a}(\nu)|^2$.

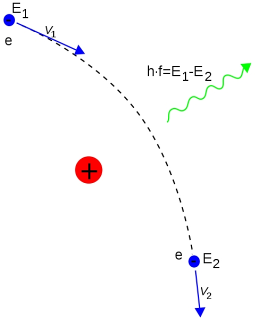

Coulombian interactions are not fully elastic because Bremsstrahlung radiation is produced when the electron is deflected by a charged particle (e.g. an ion) field, i.e. the electron is accelerated towards the target. Bremsstrahlung may be understood as the Compton scattering of a EM pulse linked to the field of the target in the electron frame.

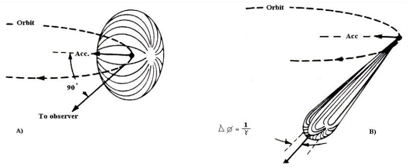

Under relativistic motion, radiation is beamed in the direction of motion of the deflected particle.

The specific power per particle is roughly $P_\nu(E) \propto \nu$ up to $h\nu \rightarrow E$, diminishing then sharply.

Timescale: $t_{\rm Br} \approx 10^6\,(\rho/m)_9^{-1}$ s

Synchrotron emission

Curved magnetic fields are carried by relativistic outflows. When spiraling and moving along the B-lines, relativistic charged particles are accelerated ($\perp$ to $\vec{v}$), and produce synchrotron radiation in the direction of $\vec{v}$. This is also understood as scattering of virtual photons.

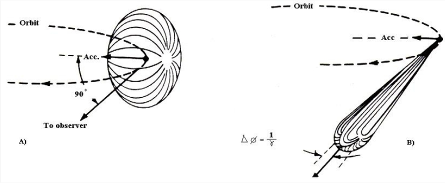

The specific power of the synchrotron radiation from a particle of energy E peaks at $\approx 0.29\, h\nu_{\rm c} \approx 20\, B_0\, E_{\rm TeV}$ keV, being $P_\nu(E) \propto \nu^{1/3}$ and $\propto \exp \nu/\nu_{\rm c}$ below and above this energy, respectively. For a particle distribution $N(E) \propto E^{-p}$, $F_\nu \propto \nu^{-\frac{p-1}{2}}$ (optically thin).

The relativistic motion induces Doppler boosting and time shortening making of an isotropic and discrete electromagnetic pulse a beamed broad spectrum radiation.

Synchrotron emission is linearly polarized, although a disordered field will smooth out the polarization signature. In AGN, the jets sometimes show strong polarization, although it is still unclear whether it has intrinsic or external (Faraday rotation) origin.

The maximum photon energy is $\sim 100\, \eta^{-1}$ MeV, where $\eta > 1$.

Timescale: $t_{\rm sy} \approx 1/a_{\rm s}\, B^2\, E \approx 390\, E_{\rm TeV}^{-1}\, B_0^{-2}$ s

Inverse Compton scattering

Accelerated electrons present in relativistic outflows can interact with synchrotron or external photons via Compton scattering. Photons get their energy boosted and acquire the electron direction in the lab frame to $O(1/\gamma)$.

In its rest frame, the electron is scattered by a photon of energy $h\nu_i'$. When $h\nu_i' \ll m_e c^2$, the electron state of motion changes very little. This is the Thomson regime. The scattered photon keeps its initial energy in the $e^{\pm}$-rest frame, but in the lab frame $h\nu_f = h\nu_f'/\gamma(1-\beta\cos\theta) \approx h\nu_i'/\gamma(1-\beta\cos\theta) \approx h\nu_i/\gamma^2(1+\beta\cos\alpha')(1-\beta\cos\theta) \sim \gamma^2 h\nu_i$. When $h\nu' \gtrsim m_e c^2$, the electron gets a significant amount of energy and momentum of the photon in its rest frame, thus implying $h\nu_f \sim \gamma m_e c^2$ in the lab frame. This is the Klein-Nishina regime. Quantum effects become important. The cross section goes from $\sim \sigma_{\rm T}$ to $\propto 1/\gamma$.

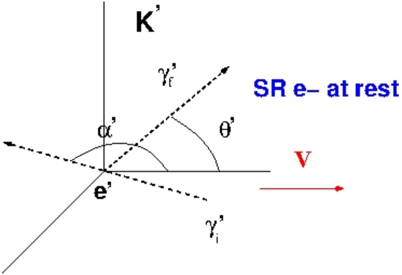

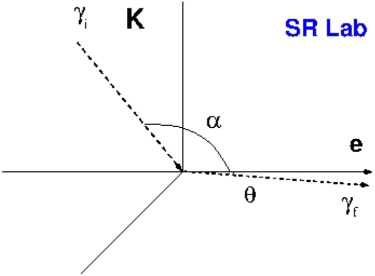

Timescale: $t_{\rm IC} \approx 100\, E_{\rm TeV}^{0.7}\, T_{4.5}^{1.7}\, u_2^{-1}$ s (KN; monoenerg.); $t_{\rm IC} \approx 63\, E_{\rm 10GeV}^{-1}\, u_2^{-1}$ s (Th)

Specific power per electron: $P_\nu(E) \propto \nu$ up to $h\nu_f$ (Th.) and $\to \delta(E)$ at $h\nu_f \sim E$ (KN)

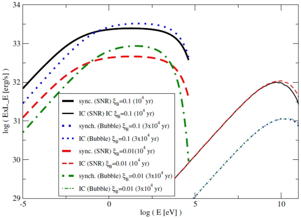

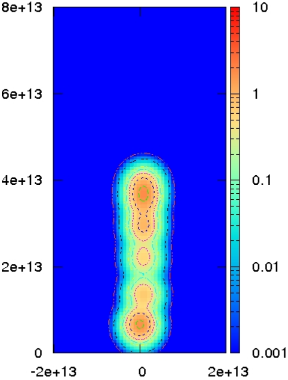

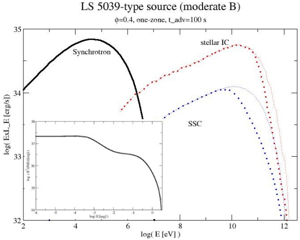

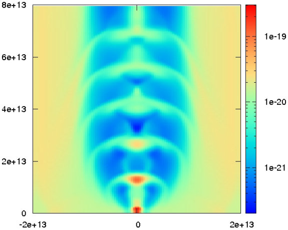

Synchrotron and inverse Compton scattering

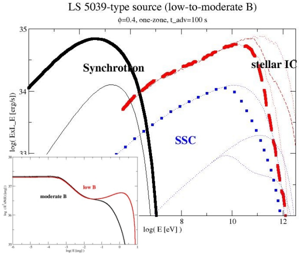

Left, top: Synchrotron and IC from a pulsar binary at large scales; bottom: density map of the axis of a jet with internal shocks. Middle: synchrotron emission from the shocked regions. Right, top: synchrotron emission with a moderate *B*-field; bottom: synchrotron and IC for two different *B*-values.

Proton-proton interactions (I)

Protons and nuclei can interact with other nuclei to produce gamma rays, $e^{\pm}$ and neutrinos mostly through the decay of π^0 and $\pi^{\pm}$. One proton or neutron is also left by the interaction. Roughly, gamma rays take $\sim E_p/6$, $\sim E_p/4$ neutrinos and $\sim E_p/12$ $e^{\pm}$; eventually $\sim E_p/2$ is converted into E-M radiation.

Each pp interaction produces a cloud of π (and other minor products) with an energy distribution strongly peaking around $\approx 0.17\,E_p$, distribution that gets softer at $E_p > 1$ TeV.

In its rest frame, π^0-decay yields two photons of equal energy and moving in opposite directions. In the emitter frame, two photons are created, one with energy $\sim E_\pi \sim E_{\rm p}/6$, and another one with a much lower energy. The gamma-ray spectrum is very hard P_ν below 67.5 MeV ($m_{\pi^0} c^2/2$), and $\propto$ to the proton spectrum above that energy; at $h\nu > 100$ GeV, the gamma-ray spectrum softens due to an increase in the π-multiplicity.

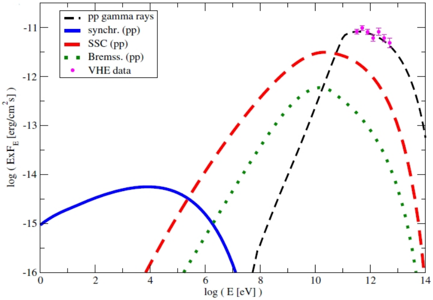

Hadronic model to explain gamma-ray flares in a non-blazar AGN through star-jet interactions. Proton acceleration and a thick target generate gamma rays as well as secondary $e^{\pm}$ synchrotron, Bremsstrahlung and synchrotron Self-Compton emission.

Timescale: $t_{\rm pp} \approx 10^6\,(\rho/m)_9^{-1}$ s

Proton-proton interactions (II)

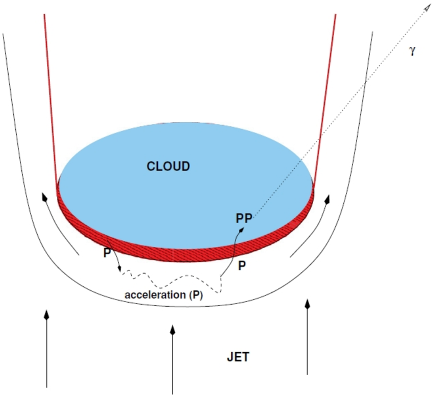

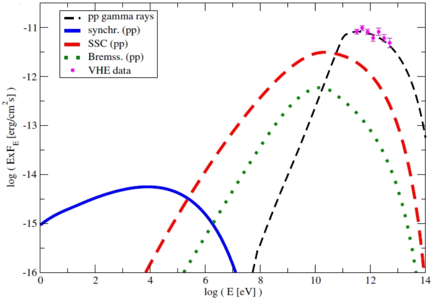

Hadronic model to explain gamma-ray flares in a non-blazar AGN through star-jet interactions. Proton acceleration and a thick target generate gamma rays as well as secondary $e^{\pm}$ synchrotron, Bremsstrahlung and synchrotron Self-Compton emission.

Proton-synchrotron

Like electrons, protons are accelerated when spiraling along the B-lines. The main difference with $e^{\pm}$-synchrotron is the emitting power, $\propto 1/m_p^4$, and the characteristic frequency $\propto 1/m_p^3$. The maximum emitting frequency can be then m_p/m_e times higher than for synchrotron photons, reaching ~ 200 GeV in the emitter frame.

Only ultrarelativistic protons under strong B-fields are efficient synchrotron emitters because of the m_p^{-4}-dependence of the emitting power. However, under certain circumstances synchrotron proton can be indeed effective. In general though, p-synchrotron is a minor cooling channel for protons.

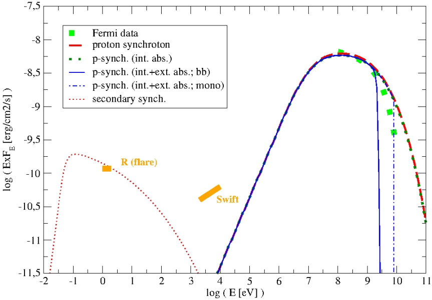

Hadronic model to explain flares in a powerful blazar AGN through star-jet interactions. Proton acceleration and a magnetized jet generate GeV photons as well as secondary $e^{\pm}$-synchrotron emission.

Timescale:

$t_{\rm sy\ p} = (m_p/m_e)^4\ t_{\rm sy} \approx 5 \times 10^5\ E_{18}^{-1}\ B_2^{-2}$ s

Other radiation / cooling processes

In the rest frame of a relativistic p, collisions with photons of energy $> 2\, m_e c^2$ and $\gtrsim m_\pi c^2$ can produce $e^\pm$ (pair creation) and $\pi^{\pm 0}$ (photomeson).

The pair-creation cross section is about 100 times larger than that of photomeson production, whereas the product-to-proton energy ratio is $\gtrsim 10^3$ times smaller. For photomeson production one has $h\nu / E_p \gtrsim 0.1$. Pions decay as in pp interactions yielding gamma rays, neutrinos and secondary $e^\pm$.

Photomeson time: $t_{\rm pm} \sim 10^8\, n_{\rm ph\,10}^{-1}$ s ($\sim$ thresh.)

The disintegration of a nucleus by impacting with photons of energy high enough to break them ($> 8\, A$ MeV in the nuclei frame; A: atomic number) leads to the nucleus destruction and the production of gamma rays and secondary nuclei.

The process is ~ 10 times more efficient than photomeson production, but the gamma ray-to-proton energy ratio is ~ 10 times smaller, implying that first the nuclei will disintegrate but still cool significantly through photomeson production.

Photo-dis. time: $t_{\rm pm} \sim 2 \times 10^{17}\, n_{\rm ph\,10}^{-1}$ s ($\sim$ thresh.)

Being charged particles, p-inverse Compton can take place, but as p-synchrotron it will be very inefficient, because of the $(m_e/m_p)^4$ reduction of the cross section.

p-inverse Compton time: $t_{\rm pic} \propto (m_e/m_p)^4\, t_{\rm IC}$

Adiabatic losses: they come from the coupling of relativistic particles and the plasma; i.e. relativistic particles make work!

Phenomenology: gains and losses

Acceleration time: (criterion: $A_i = 10^i$ in cgs units unless otherwise stated)

$t_{\rm acc} = \eta\, r_{\rm g}/c \approx 0.1\eta\, E_{\rm TeV}\, B_0^{-1}$ s; $\eta \geq 1$ is the acceleration efficiency ($\eta = 1$: limiting case)

Cooling/escape times (relevant to acceleration):

Synchrotron: $t_{\rm sy} = 1/a_{\rm s}\, B^2\, E \approx 390\, E_{\rm TeV}^{-1}\, B_0^{-2}$ s

Inverse Compton: $t_{\rm IC} \approx 100\, E_{\rm TeV}^{0.7}\, T_{4.5}\, u_2^{-1}$ s (KN; monoenerg.); $t_{\rm IC} \approx 60\, E_{\rm 10GeV}^{-1}\, u_2^{-1}$ s (Th)

Dynamical time (escape, adiabatic cooling): $t_{\rm dy} \sim l/v = 100\, l_{12}\, v_{10}^{-1}$ s

Diffusion (escape): $t_{\rm diff} = l^2/2\,D \approx 15000\, B_0\, l_{12}^2\, E_{\rm TeV}^{-1}\, \chi^{-1}$ s ($D = \lambda\, c/3 = \chi\, r_{\rm g}\, c/3$)

Low energies (relevant to acceleration):

Ionization/coulombian losses: $t_{\rm ion/c} \approx 2 \times 10^{18}\, E_{\rm GeV}\, (\rho/m)_9^{-1}$ s

Phenomenology: maximum energies

Rate balance ($t_{acc} = t_{cool}$) yields, depending on the dominant process:

Synchrotron: $E_{max}^{sy} = 60\,\eta^{-1/2}\,B_0^{-1/2}$ TeV

Inv. Comp.: $E_{max}^{IC} \approx 10^{10}\,(B_0\,T_{4.5}\,u_2^{-1}\,\eta^{-1})^{3.3}$ TeV (KN; monoen.); $E_{max}^{IC} = 2500\,B_0^{1/2}\,u_2^{-1/2}\,\eta^{-1/2}$ GeV (Th)

Dynamical time (escape, adiabatic cooling): $E_{max}^{dy} \sim 910\,R_{12}\,B_0\,v_{10}^{-1}\,\eta^{-1}$ TeV

Diffusion: $E_{max}^{diff} = 370\,R_{12}\,B_0\,\eta^{-1/2}\,\chi^{-1/2}$ TeV

Electrons are strongly affected by synchrotron cooling, but losing energy through exerting work (adiabatic losses) or diffusing out of the source cannot be neglected. Coulombian collisions should not prevent acceleration to start either. Protons are most likely affected by adiabatic losses or diffusive escape. Only under very specific conditions of size and magnetic, matter or radiation fields, Bremsstrahlung, proton-proton interactions, proton-synchrotron or photomeson production limit the energy of the particles.

Outline

Pair creation and gamma-ray absorption

In the center of momentum frame, two photons can create a $e^{\pm}$-pair if $\epsilon_{1,2\ \mathrm{CM}} > m_e c^2$.

The pair opacity is $\tau = \sigma_{\gamma\gamma} n_{\mathrm{ph}} l \approx 0.3\ n_{\mathrm{ph}\ 12} l_{12.5}$, and the pair luminosity can be estimated as:

$\propto (1 - \exp^{-\tau}) L_\gamma^{>th} \sim (1 - \exp^{-0.3\ n_{\mathrm{ph}\ 12} l_{12.5}}) L_\gamma^{>th}$

The Energy threshold of pair creation is $\epsilon_{\gamma\mathrm{th}} \sim 2/\epsilon_*(1 - \cos\theta) \sim 1/\epsilon_*\ (m_e c^2)$, which depends on the two-photon interaction angle; $\epsilon_{\gamma\mathrm{th}}$ roughly corresponds to the pair distribution maximum. The smaller the θ-value, the higher the photon energies that are required in the lab frame.

The interaction probability is $\propto (1 - \cos\theta)$, so most of pairs are generated toward the target source.

Pair creation under a UV photon field

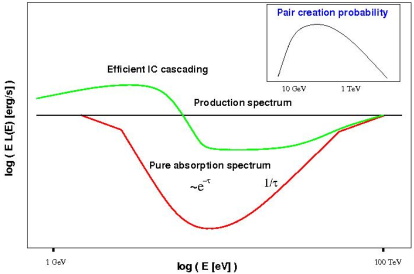

The minimum energy one pair member has is $E \sim \epsilon_{\gamma\mathrm{th}}$, and the maximum, $E \to \epsilon_\gamma$. Close to the threshold, both $e^{\pm}$ have similar energies, differing more and more the higher the energy.

The inverse Compton cascade

Pairs follow a distribution similar to that of gamma rays for $E > \epsilon_{\gamma\mathrm{th}}$ when $\tau(\epsilon_\gamma) > 1$, and for $\tau < 1$ become softer by $\sim 1/E$ well above $\epsilon_{\gamma\mathrm{th}}$. For anisotropic photon fields, the spectrum is not uniform. Depending on the cooling mechanism, absorption has different effects on the broadband emission.

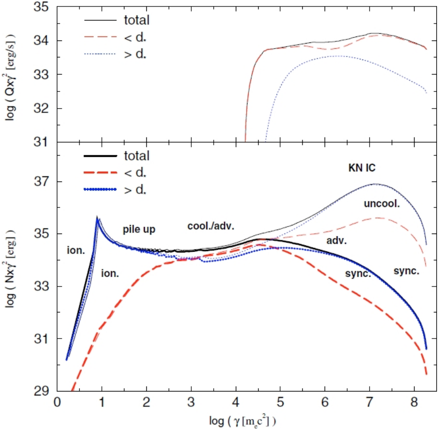

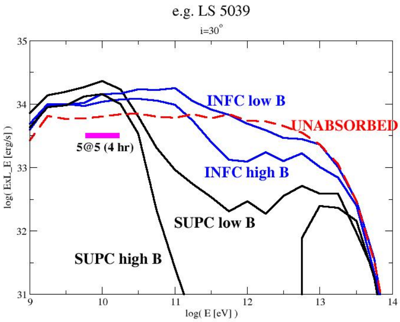

When the dominant cooling process is inverse Compton scattering, the $e^{\pm}$ produce gamma rays of similar energy that can be absorbed again producing more pairs. This triggers the so-called IC-cascade. Absorption takes place, but energy is reprocessed but still released at high energies.

The synchrotron channel

For high enough B-fields synchrotron losses for $e^{\pm}$ with $E > \epsilon_{\gamma\mathrm{th}}$ become dominant. However, the IC-cascade is only efficient when $E \gtrsim$ few times $\epsilon_{\gamma\mathrm{th}}$.

When the IC-cascade is important inverse Compton takes place in Klein Nishina, so even weak magnetic fields can channel most of the emission through synchrotron radiation at high energies. IC takes place then mostly through single scattering. Other cooling channels like relativistic Bremsstrahlung or adiabatic losses may be important, but at lower energies.

Gamma-ray reprocessing is important in compact sources (e.g. close binary systems) or in very far objects (e.g. in AGN, through VHE or UHE gamma-ray interactions with EBL or CMB).

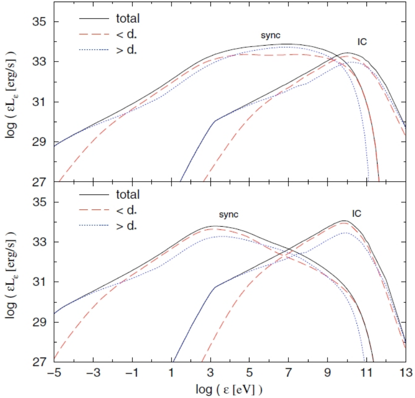

Synchrotron and IC for two different gamma-ray spectra (hard: top; soft: bottom) and a moderate B-field. The two contributions are comparable.

X-ray absorption

X-rays suffer absorption mainly through the photo-electric effect. The opacity has a strong dependence on energy, being the strongest at low energies.

The E^3-weighted cross section under solar abundances:

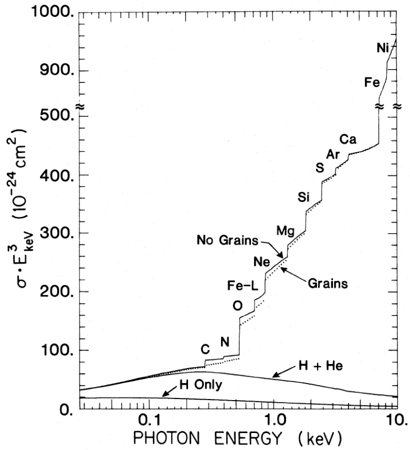

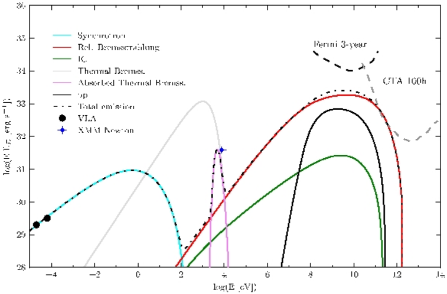

Impact on the UV and X-ray energy bands of a high-density medium in which the emitter of a certain size is embedded.

Within a factor of two, in the energy range $\gtrsim$ 1 keV, the opacity is $\tau_{\rm ph} \sim 20\, N_{23} (h\nu)^{-2.5}_{\rm keV}$.

Radio absorption

Radio photons interact effectively through free-free absorption with plasma free electrons (*inverse* Bremsstrahlung), with a strong dependence on density, source size and temperature. The opacity of the process can be written approximately as

free-free abs,: $\tau_{\rm ff} \sim 0.75 \times T_5^{-1.5} \nu_{\rm GHz}^{-2} n_5 l_{16}$

The plasma refraction coefficient changes for long wavelengths, reducing the transmission efficiency at low frequencies: the Tsytovitch-Razin effect. This produces a low-energy cutoff in the radiation spectrum. The ionization level is also relevant. In frequency, this cutoff is located at

Tsytovitch-Razin abs.: $\nu_{\rm TR} = 2 \times 10^7 n_5 B_0^{-1}$ **GHz**

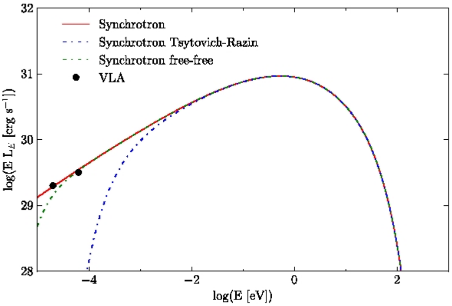

Impact on the radio spectrum at low frequencies of a high-density medium in which relativistic electrons radiate synchrotron emission.

Synchrotron-emitting electrons easily absorb radio photons of a frequency similar to that produced by them, with a strong dependence on the relativistic electron density, source size, and the magnetic field. The frequency below which absorption begins is: **synch. self-abs.:** $\nu_{\rm max} \approx 10\, F_{\rm max\ mJy}^{2/5} B_0^{1/5} R_{12}^{-4/5}$ **GHz**

Outline

Summarizing...

Non-thermal radiation is very sensitive to plasma conditions, and so bring us information from extreme regions of the Universe. Relativistic outflows are produced in, and are themselves among, the fastest and hottest plasmas, being generated in the deepest gravitational wells.

Collapsed objects are the engines of relativistic outflows of any type, being gravity the main source of energy and *B*-fields the mediators of their generation, the propagation, and the collective processes occurring on them.

Through dynamical and radiative interactions, the rich environment of relativistic outflows is affected by and gives as information about them. Several disciplines concur if relativistic outflows are to be properly studied.

Being possible only since recently, detailed studies of relativistic outflows and associated non-thermal processes allow an insight into physical conditions and mechanisms that cannot be probed in the laboratory, representing a large novel window for our understanding of the Universe.